Capacity of entanglement and the distribution of density matrix eigenvalues in gapless systems

Yuya O. Nakagawa[1,*] and Shunsuke Furukawa[2]

[1]*Institute for Solid State Physics, University of Tokyo, 5-1-5 Kashiwanoha, Kashiwa, Chiba 277-8581, Japan*

[2]*Department of Physics, University of Tokyo, 7-3-1 Hongo, Bunkyo-ku, Tokyo 113-0033, Japan*

(Received 6 September 2017; published 7 November 2017)

We propose that the properties of the capacity of entanglement (COE) in gapless systems can efficiently be investigated through the use of the distribution of eigenvalues of the reduced density matrix (RDM). The COE is defined as the fictitious heat capacity calculated from the entanglement spectrum. Its dependence on the fictitious temperature can reflect the low-temperature behavior of the physical heat capacity and thus provide a useful probe of gapless bulk or edge excitations of the system. Assuming a power-law scaling of the COE with an exponent α at low fictitious temperatures, we derive an analytical formula for the distribution function of the RDM eigenvalues. We numerically test the effectiveness of the formula in a relativistic free scalar boson in two spatial dimensions and find that the distribution function can detect the expected $\alpha = 3$ scaling of the COE much more efficiently than the raw data of the COE. We also calculate the distribution function in the ground state of the half-filled Landau level with short-range interactions and find better agreement with the $\alpha = 2/3$ formula than with the $\alpha = 1$ one, which indicates a non-Fermi-liquid nature of the system.

DOI: 10.1103/PhysRevB.96.205108

I. INTRODUCTION

Quantum entanglement, which represents nonlocal correlations that cannot be described by classical mechanics, has played a central role in quantum information science and has recently become an indispensable tool in studies of quantum many-body systems. One can extract various properties of a system by calculating entanglement measures in the many-body (mostly, ground-state) wave function $|\Psi\rangle$ [1,2]. The most celebrated measure among them is the entanglement entropy (EE). By partitioning the system into a subregion A and its complement $\bar{A}$, the EE is defined as the von Neumann entropy $S_A := -\mathrm{Tr}\rho_A \ln \rho_A$ of the reduced density matrix (RDM) $\rho_A := \mathrm{Tr}_{\bar{A}}|\Psi\rangle\langle\Psi|$. When the ground state $|\Psi\rangle$ contains only short-range correlations, the EE scales with the boundary size of A (boundary law) [3,4]. Deviation from a boundary law signals the presence of certain nontrivial correlations and can furthermore reveal universal numbers characterizing the system. In one-dimensional (1D) quantum critical systems, for example, the EE for an interval of length x shows a logarithmic scaling $S_A = \frac{c}{3}\log\frac{x}{a}$, where c and a are the central charge and the (nonuniversal) short-distance cutoff of underlying conformal field theory (CFT) [5–8]. In noninteracting fermions and Fermi liquids in general dimensions, the EE can detect a Fermi surface through a multiplicative logarithmic correction to a boundary law [9–14]. Interestingly, the EE can also detect a hidden Fermi surface of emergent particles (such as spinons and composite fermions) in a similar manner [15–20], providing a guiding principle for constructing a holographic dual of a strongly interacting metal [21,22]. In topologically ordered systems [23–26] and in some two-dimensional critical systems [27–29], the EE obeys a boundary law, but there appears a subleading universal constant that reflects underlying topological or critical properties. While the EE was initially featured on the theoretical side, state-of-the-art techniques in ultracold atomic systems can now measure it experimentally [30–32], fostering further growing interest among both theorists and experimentalists.

Since the EE can be calculated from the eigenvalues of the RDM, the latter can, in principle, contain more information of the system than the former. This idea has led to the notion of entanglement spectrum (ES) [33]. By rewriting the RDM in the thermal form $\rho_A = e^{-H_E}$, where H_E is referred to as the entanglement Hamiltonian, the ES is defined as the full eigenvalue spectrum of H_E. Although the ES is calculated from the ground state, a number of studies have demonstrated that the ES resembles the physical energy spectrum of the system. In gapped topological phases, in particular, the ES has been found to exhibit the same low-energy features as the physical edge-mode spectrum [23,33–39]. Several physical "proofs" have been given for this remarkable correspondence [40–45], while some exceptions to it have also been discussed [46,47].

The correspondence between the ES and the physical spectrum has also been found in some gapless systems. In 1D critical systems, beautiful numerical evidence has been presented for the correspondence between the ES and the energy spectrum of a boundary CFT [48]. In systems with spontaneous continuous symmetry breaking, the ES has been found to exhibit a tower structure in a way analogous to the physical spectrum [49–51]. In gapless phases of spin ladders, however, the ES between the chains has been found to exhibit a flat or fractional dispersion relation as opposed to a linear energy dispersion of a single chain [44,52].

To gain further insights into the properties of the ES, it is useful to look into the "thermodynamics" of the entanglement Hamiltonian H_E. The capacity of entanglement (COE) has been introduced for such a purpose [35,53–56]. The COE $C_E(T_E)$ is defined as the fictitious heat capacity of H_E, where T_E is the fictitious temperature (see Sec. II for a precise definition of the COE). The correspondence between the ES and the physical spectrum can then be revealed by the correspondence between the COE and the physical heat capacity. In 1D critical systems, the CFT prediction $\mathrm{Tr}\rho_A^n \sim (x/a)^{\frac{c}{6}(n-1/n)}$ [5,7,8] leads to a linear scaling $C_E \sim T_E$

*y-nakagawa@issp.u-tokyo.ac.jp

[56,57], which coincides with the low-temperature behavior of the physical heat capacity [58]. Noninteracting fermions and Fermi liquids with a Fermi surface can be described as a collection of CFTs [11–13], and thus, the COE of these systems is also expected to show a linear scaling $C_E \sim T_E$ at low T_E as the physical heat capacity does. In more general gapless systems, the correspondence between the COE and the physical heat capacity is unclear, and some counterexamples to the correspondence are known [56]. However, one can still use the COE to probe unusual low-energy properties of the system. For example, based on the above consideration, a non-Fermi-liquid behavior can be signaled by the violation of the linear scaling of the COE (see also Ref. [17] for a related discussion). This indicates an advantage of the COE over the EE as the latter does not seem to distinguish Fermi and non-Fermi liquids in a qualitative manner [15,16,18,19]. Furthermore, the COE has an advantage over the physical heat capacity in that the former requires only the ground-state wave function and can be applied to a trial wave function.

In this paper, we investigate the behaviors of the COE and the distribution of the ES (more precisely, the distribution of the RDM eigenvalues) in some gapless systems. We find that a nontrivial low-T_E behavior of the COE can efficiently be detected through the use of the distribution of the ES. Specifically, by assuming a power-law behavior $C_E \sim T_E^\alpha$ at low T_E, we derive an analytic formula for the cumulative distribution function $n(\lambda)$ of the RDM eigenvalues [see Eq. (8) below]. This is based on a generalization of the work by Calabrese and Lefevre for 1D critical systems [59]. We numerically test the effectiveness of the formula in a relativistic free scalar boson in two spatial dimensions and find that $n(\lambda)$ can detect the expected $\alpha = 3$ scaling of the COE much more efficiently than the raw data of the COE. This advantage of $n(\lambda)$ results from a sensitive dependence of the analytic formula (8) on α. As a more nontrivial application, we then study the half-filled Landau level with short-range interactions. For this system, Halperin, Lee, and Read (HLR) [60] formulated a theory of a Fermi sea of composite fermions (see also Refs. [61–68] for recent interesting theoretical developments on this system). Gauge fluctuations in the HLR theory were shown to make a singular contribution to heat capacity, which scales as $T^{2/3}$ if the bare interaction between fermions is short range [60,69]. We have calculated $n(\lambda)$ of this system by using the ground state obtained by exact diagonalization and have found better agreement with the $\alpha = 2/3$ formula than with the $\alpha = 1$ one, which indicates a non-Fermi-liquid nature. While our data obtained for maximally $N = 14$ particles do not allow precise determination of α, relatively good agreement with the $\alpha = 2/3$ formula suggests an intriguing possibility that the correspondence between the ES and the physical spectrum still holds in a strongly interacting metallic state.

The rest of this paper is organized as follows. In Sec. II, we derive the analytical formula for the distribution of the RDM eigenvalues by assuming a power-law behavior of the COE. In Sec. III, we present numerical results in a free scalar boson and the half-filled Landau level. In Sec. IV, we conclude the paper and discuss the implications of our study.

II. CAPACITY OF ENTANGLEMENT AND DISTRIBUTION OF DENSITY MATRIX EIGENVALUES

In this section, we first describe the definitions of the COE and the distribution of the RDM eigenvalues. We then derive an analytic formula for the distribution of the RDM eigenvalues by assuming a power-law behavior of the COE, $C_E \sim T_E^\alpha$, at low T_E.

A. Definitions

Let us first clarify the definitions of the COE and the distribution of the RDM eigenvalues. Using the RDM $\rho_A = e^{-H_E}$ on a subregion A, we introduce the entanglement partition function as

$$Z_E(T_E) := \mathrm{Tr} e^{-H_E/T_E} = \mathrm{Tr}\rho_A^{1/T_E}. \tag{1}$$

The COE is then defined as [35,53,56]

$$C_E(T_E) := T_E \frac{\partial^2}{\partial T_E^2}[T_E \ln Z_E(T_E)]. \tag{2}$$

In the above expressions, we dropped the dependence on A as it is not considered throughout our analysis. We are instead interested in the dependence on the fictitious temperature T_E. As the entanglement Hamiltonian H_E is dimensionless, T_E is too. We note that studying the dependence of the COE on T_E is equivalent to studying the Rényi EE

$$S_n := \frac{-1}{n-1} \ln R_n, \quad R_n := \mathrm{Tr}\rho_A^n = Z_E(1/n)$$

as a function of the Rényi parameter n.

Next we introduce the distribution of the RDM eigenvalues. We denote the eigenvalues of the RDM ρ_A by $\{\lambda_i\}$. Since ρ_A is positive semidefinite and has unit trace, these eigenvalues satisfy $0 \leqslant \lambda_i \leqslant 1$ and $\sum_i \lambda_i = 1$. The distribution function $P(\lambda)$ and the cumulative distribution function $n(\lambda)$ of $\{\lambda_i\}$ are defined as [59]

$$P(\lambda) := \sum_i \delta(\lambda - \lambda_i), \quad n(\lambda) := \int_\lambda^{\lambda_{\max}} P(\lambda) d\lambda, \tag{3}$$

where $\lambda_{\max}$ is the largest eigenvalue. Here, $n(\lambda)$ counts the number of eigenvalues in the range $[\lambda,\lambda_{\max}]$. If $\{\lambda_i\}$ is sorted in descending order ($\lambda_1 = \lambda_{\max} \geqslant \lambda_2 \geqslant \lambda_3 \geqslant \ldots$), $n(\lambda)$ can also be viewed as the inverse function of λ_i.

B. Derivation of an analytic formula

By assuming $C_E \sim T_E^\alpha$ with $\alpha > 0$ at low T_E, we now derive an analytic formula for the cumulative distribution function $n(\lambda)$. Our derivation is based on a generalization of the argument by Calabrese and Lefevre for 1D critical systems [59] where $C_E \sim T_E$ at low T_E (see also Refs. [70,71] for related works on the "negativity spectrum").

Since $Z_E(T_E)$ is related to the COE via Eq. (2), our assumption about the COE immediately leads to

$$\ln Z_E(T_E) = bT_E^\alpha + b' + b''/T_E,$$

where b, b', and b'' are constants. One can determine these constants by using some properties of $Z_E(T_E)$. In the limit $T_E \to 0$, the definition of $Z_E(T_E)$ in Eq. (1) yields

$Z_E(T_E) \to \lambda_{\max}^{1/T_E}$, which indicates $b' = 0$ and $b'' = \ln \lambda_{\max}$. By further using $Z_E(T_E = 1) = \mathrm{Tr}\rho_A = 1$, we find $b = -b'' = -\ln \lambda_{\max}$. We thus obtain a simple form,

$$\ln Z_E(T_E) = b(T_E^\alpha - 1/T_E), \quad b = -\ln \lambda_{\max}. \tag{4}$$

Following Ref. [59], we introduce the function

$$f(z) := \frac{1}{\pi} \sum_{n=1}^{\infty} R_n z^{-n} = \frac{1}{\pi} \int d\lambda' \frac{\lambda' P(\lambda')}{z - \lambda'}. \tag{5}$$

Here, the middle expression converges only for $|z| > \lambda_{\max}$, while the rightmost expression is analytic except in the interval $0 \leqslant z \leqslant \lambda_{\max}$ on the real axis. Adopting the rightmost expression as the analytic continuation of the middle one, the distribution function $P(\lambda)$ can be obtained as $\lambda P(\lambda) = \lim_{\epsilon \to +0} \mathrm{Im} f(\lambda - i\epsilon)$. By using Eq. (4), we can calculate $f(z)$ as

$$\begin{aligned} f(z) &= \frac{1}{\pi} \sum_{n=1}^{\infty} e^{b(1/n^\alpha - n)} z^{-n} \\ &= \frac{1}{\pi} \sum_{n=1}^{\infty} \left(\frac{\lambda_{\max}}{z} \right)^n \sum_{k=0}^{\infty} \frac{1}{k!} \left(\frac{b}{n^\alpha} \right)^k \\ &= \frac{1}{\pi} \sum_{k=0}^{\infty} \frac{b^k}{k!} \mathrm{Li}_{\alpha k}(\lambda_{\max}/z), \end{aligned} \tag{6}$$

where $\mathrm{Li}_m(y) = \sum_{n=1}^{\infty} y^n/n^m$ is the polylogarithm function. While the power series expression of $\mathrm{Li}_m(y) (m \geqslant 0)$ converges only for $|y| < 1$, it has an analytic continuation for $|y| \geqslant 1$; it then has a branch cut on the real axis for $y \geqslant 1$ with the discontinuity

$$\lim_{\epsilon \to +0} \mathrm{Li}_m(y + i\epsilon) - \mathrm{Li}_m(y) = \begin{cases} i\pi \frac{(\ln y)^{m-1}}{\Gamma(m)} & (m > 0), \\ i\pi \delta(1 - y) & (m = 0), \end{cases} \tag{7}$$

as noted in Ref. [59]. Therefore, by taking the limit $z \to \lambda - i0$ in Eq. (6), we obtain

$$\lambda P(\lambda) = \lambda_{\max} \delta(\lambda - \lambda_{\max}) + \Theta(\lambda_{\max} - \lambda) \sum_{k=1}^{\infty} \frac{b^k \Lambda^{\alpha k - 1}}{k!\, \Gamma(\alpha k)},$$

where $\Lambda = \ln(\lambda_{\max}/\lambda)$ and $\Theta(x)$ is the Heaviside step function. By integrating $P(\lambda)$, we arrive at the formula

$$n(\lambda) = 1 + \sum_{k=1}^{\infty} \frac{\{b[\ln(\lambda_{\max}/\lambda)]^\alpha\}^k}{k! \Gamma(\alpha k + 1)}, \tag{8}$$

which plays a central role in this paper. Although this formula is expressed as an infinite series, it can be evaluated numerically for a given $\alpha > 0$ as it converges rapidly. When $\alpha = 1$, the infinite series can be rewritten as the modified Bessel function, resulting in the formula of Calabrese and Lefevre [59]. We note that when α is a rational number, $n_\alpha(\lambda)$ can be written as a sum of the generalized hypergeometric functions (see Appendix A).

III. NUMERICAL RESULTS

In this section, we present numerical results of the COE $C_E(T_E)$ and the cumulative distribution function $n(\lambda)$ of the RDM eigenvalues in some gapless systems. We first test the effectiveness of formula (8) in a relativistic free scalar boson in two spatial dimensions. Then, as a more nontrivial application, we present an exact diagonalization result in the half-filled Landau level with short-range interactions. By comparing the numerical data with formula (8), we find a signature of the non-Fermi-liquid nature of this system.

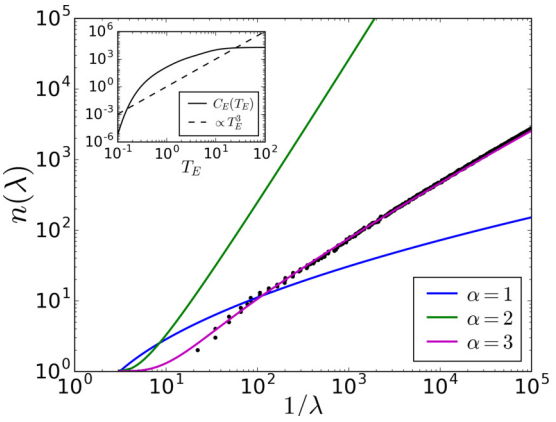

FIG. 1. Cumulative distribution function $n(\lambda)$ of the RDM eigenvalues in a relativistic free scalar boson in two spatial dimensions. In numerical calculations, we discretized the field theory and took as the subregion A a circle with a radius of 10 discretized units. Lines indicate the analytic formula (8) for three different values of the exponent α. We find good agreement of the numerical data with the $\alpha = 3$ formula. The inset shows the COE $C_E(T_E)$ (solid line) in comparison with the expected low-T_E scaling $C_E \propto T_E^3$ [56] (dashed line).

A. Relativistic free scalar boson in two spatial dimensions

Building on the analytic expression of the Rényi EE obtained by Klebanov *et al.* [72], Nakaguchi and Nishioka [56] calculated the COE of a relativistic massless free scalar boson. In two spatial dimensions, in particular, the COE has been shown to scale as $C_E \sim T_E^3$ at low T_E. Interestingly, this is different from the low-T behavior of the physical heat capacity $C \sim T^2$, providing a counterexample to the correspondence between the two quantities.

An advantage of this system for testing formula (8) is the availability of an efficient numerical technique for computing the RDM eigenvalues. Following Ref. [73], we discretize the field theory of the scaler boson ϕ with the action

$$S = \int d^2x dt [(\partial_t \phi)^2 - (\nabla \phi)^2] \tag{9}$$

and calculate the RDM eigenvalues by taking as a subregion A a circle centered at the origin. Further technical details of the numerical calculation are described in Appendix B.

Figure 1 presents the cumulative distribution function $n(\lambda)$ and the COE $C_E(T_E)$ (inset) calculated numerically. It is clear that the data for $n(\lambda)$ agree well with the analytic formula (8) with $\alpha = 3$, as expected. In contrast, the data for $C_E(T_E)$ plotted in logarithmic scales show a significant variation of slope; estimation of α through the fitting with the form $C_E \sim T_E^\alpha$ would crucially depend on the range of T_E used for the fitting. These results indicate an advantage of $n(\lambda)$ over the

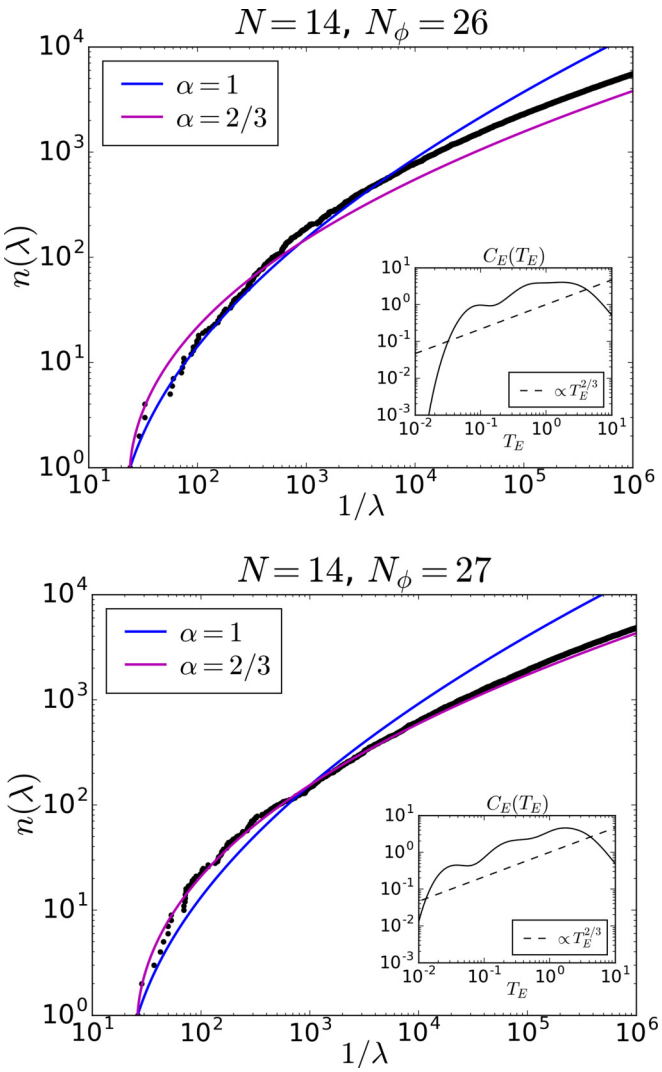

FIG. 2. Cumulative distribution function $n(\lambda)$ of the RDM eigenvalues for the ground state of the half-filled Landau level (dots) in comparison with the analytic formula (8) for $\alpha = 2/3$ and $\alpha = 1$ (lines). The top and bottom panels correspond to the Fermi sea case ($N_\phi = 2N - 2$) and the particle-hole symmetric case ($N_\phi = 2N - 1$), respectively, where N is set to 14. In plotting the analytical formula, the numerically obtained value of $\lambda_{\max}$ is used. The insets show the COE $C_E(T_E)$ (solid line) in comparison with the power-law behavior $C_E \propto T_E^{2/3}$ (dashed line).

COE $C_E(T_E)$ in determining the exponent α. This advantage results from a sensitive dependence of formula (8) on α.

B. Half-filled Landau level

As a more nontrivial application of our formula (8), we consider a quantum Hall system at the filling factor $\nu = 1/2$ (half-filled Landau level). For this system, HLR formulated an effective field theory in which composite fermions form a Fermi sea and interact via a Chern-Simons gauge field [60]. Gauge fluctuations in this theory were shown to make a singular contribution to heat capacity [60,69]. In particular, when the bare interaction between fermions is short range, the heat capacity is predicted to scale as $C \sim T^{2/3}$, indicating a non-Fermi-liquid behavior. However, this prediction has not been verified numerically as a large number of low-lying eigenenergies are required to obtain low-temperature behavior of the heat capacity. Recently, there have been very active studies on the role of particle-hole symmetry in this system. The HLR theory does not satisfy this symmetry, and an alternative description in terms of Dirac composite fermions consistent with this symmetry has been developed [63–67]. In this description, Dirac composite fermions have a Fermi surface and interact via a gauge field without a Chern-Simons term. While the heat capacity has not been calculated in the Dirac scenario, the gauge field coupled with a Fermi surface is still expected to make a significant contribution.

Concerning entanglement properties, the $n = 2$ Rényi EE has recently been calculated for trial wave functions of the half-filled Landau level, and a multiplicative logarithmic correction to the boundary law, which indicates a hidden Fermi surface, has been verified [18,19] (see also Refs. [53,74] for entanglement in related systems). However, the Rényi EE for fixed n could not reveal a non-Fermi-liquid nature of the system. This motivates us to investigate the COE and the distribution of RDM eigenvalues in this system.

We performed an exact diagonalization calculation for interacting N spinless fermions in the lowest Landau level in a spherical geometry [75]. In this geometry, a magnetic monopole of charge N_ϕ in units of the flux quantum h/e is placed at the center. We assume a repulsive short-range interaction $V(\boldsymbol{r}) = -\nabla^2\delta(\boldsymbol{r})$ between fermions; this interaction is equivalent to Haldane's pseudopotential for the $\nu = 1/3$ Laughlin state [75,76], while we here focus on the filling $\nu = 1/2$. A Fermi sea of composite fermions corresponds to a set of (N, N_ϕ) satisfying $N_\phi = 2N - 2$ [77], whereas the particle-hole symmetric state (with a possible Dirac nature) is consistent with those satisfying $N_\phi = 2N - 1$ [63]. We investigate both types of states in numerical calculations; in the thermodynamic limit, they both correspond to the filling factor $\nu = 1/2$. The ground state is $(2L + 1)$-fold degenerate if it has a total angular momentum of magnitude $L > 0$; in such a case, we took the ground state in the $L_z = 0$ or $1/2$ sector for the computation of the RDM, where L_z is the z component of the total angular momentum. From such a ground state, we calculated the eigenvalues of the RDM associated with the real space cut into two hemispheres [38,39].

Figures 2 and 3 present the cumulative distribution function $n(\lambda)$ and the COE $C_E(T_E)$ (inset of Fig. 2) obtained in this way. In Fig. 2, we compare the numerical data of $n(\lambda)$ for $N = 14$ with the analytic formulas with $\alpha = 2/3$ and $\alpha = 1$. The numerical data clearly show better agreement with the $\alpha = 2/3$ formula than with the $\alpha = 1$ one, in both the Fermi sea case ($N_\phi = 2N - 2$) and the particle-hole symmetric case ($N_\phi = 2N - 1$). The data for $C_E(T_E)$ plotted in logarithmic scale again show a variation of slope, although a rough agreement with $\alpha = 2/3$ is found for $10^{-1} \lesssim T_E \lesssim 10^0$. We furthermore compare the results for different N in Fig. 3. One can see that the data for $n(\lambda)$ tend to approach the analytic formula with $\alpha = 2/3$ with increasing N, although a marked deviation from the formula is found for $(N, N_\phi) = (12, 22)$. We infer that this deviation originates primarily from the spatial inhomogeneity of the fermion density around the boundary of the subregion A. When the ground state has a nonzero magnitude of the angular

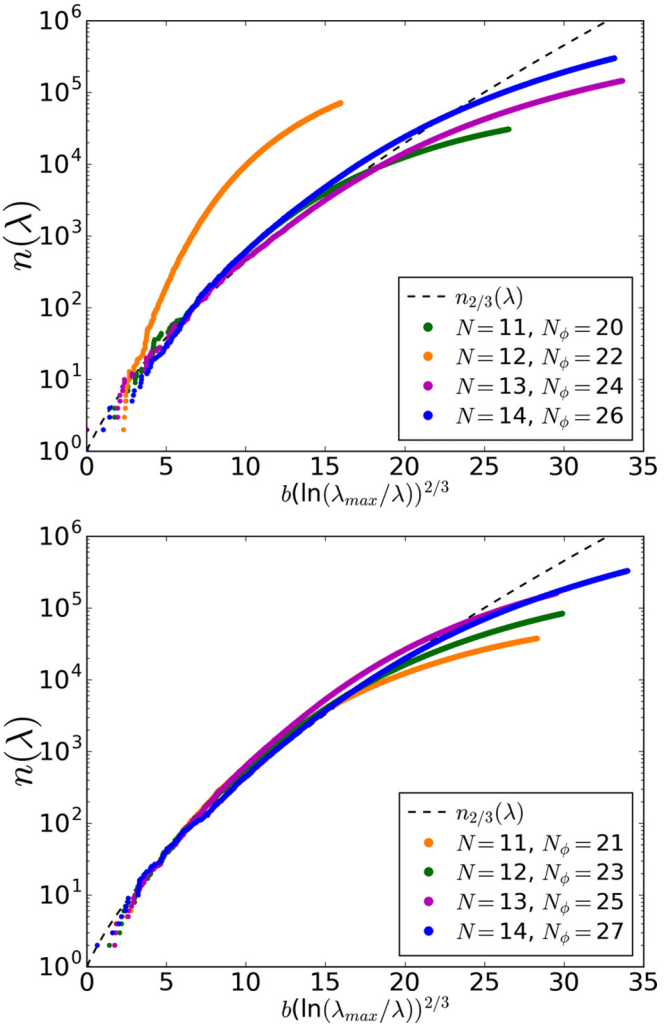

FIG. 3. Cumulative distribution function $n(\lambda)$ for the ground state of the half-filled Landau level for different N. Numerical results (colored dots) are compared with the analytic formula (8) with $\alpha = 2/3$ (dashed line). The top and bottom panels correspond to the Fermi sea case ($N_\phi = 2N - 2$) and the particle-hole symmetric case ($N_\phi = 2N - 1$), respectively.

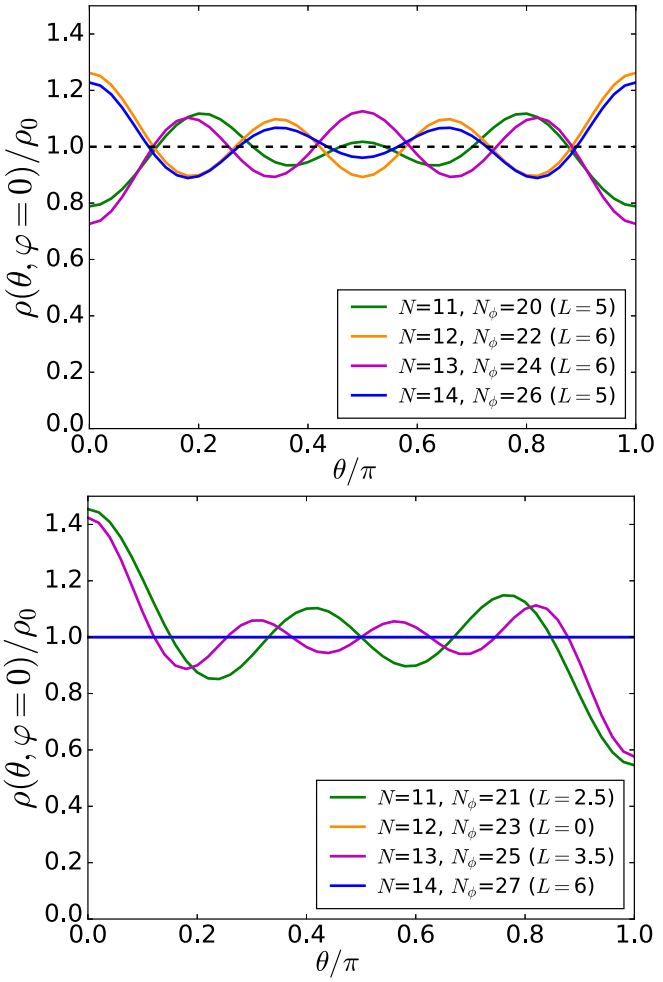

FIG. 4. Density of fermions in the ground state of the half-filled Landau level in the cases examined in Fig. 3. The density $\rho(\theta,\varphi)$ is normalized by the average density $\rho_0 = N/S$, where S is the area of the sphere. The dashed line in the top panel indicates the case of homogeneous density as a guide for the eye. In the bottom panel, the data for $N = 12$ and 14 are overlapping.

momentum $L > 0$, the $L_z = 0$ state used in our calculations can exhibit an inhomogeneous density that depends on the azimuthal angle θ (but not on the polar angle φ because of the axial symmetry), as displayed in Fig. 4. The ground states for $(N,N_\phi) = (12,22)$ and $(13,24)$ in the Fermi sea case have comparatively large L, and as seen in Fig. 4, show appreciable deviations of the density from the average value at the boundary of A ($\theta = \pi/2$, the equator of the sphere). Therefore, these states can exhibit large finite-size effects; owing to their nonuniversal nature, such effects are prominent only for $(N,N_\phi) = (12,22)$ in Fig. 3. In the particle-hole symmetric case (Fig. 4, bottom), because of a unique antisymmetric behavior, the deviation of the density from the average value vanishes at the boundary of A, which may explain smaller finite-size effects than in the Fermi sea case, as seen in Fig. 3.

Despite the tendency of the numerical data to approach the $\alpha = 2/3$ formula in Fig. 3, it is worth checking further whether our data obtained for maximally $N = 14$ particles really capture the behavior of the distribution function $n(\lambda)$ in the thermodynamic limit. This can be done by, e.g., examining the robustness of the results for different geometries (such as a torus) and different interactions. It would also be interesting if the distribution function $n(\lambda)$ could be calculated in larger systems by using a density matrix renormalization group [66] or by developing an efficient method based on trial wave functions.

IV. CONCLUSIONS

In this paper, we have studied the COE $C_E(T_E)$ and the cumulative distribution function $n(\lambda)$ of RDM eigenvalues in gapless systems. Assuming a power-law behavior $C_E \sim T_E^\alpha$ at low T_E, we have derived an analytic formula of $n(\lambda)$ as in Eq. (8). We have numerically tested the effectiveness of the formula in relativistic free scalar bosons in two spatial dimensions and have found that the distribution of RDM eigenvalues can detect the expected $\alpha = 3$ scaling of the COE much more efficiently than the raw data of the COE. We have also calculated the distribution of RDM eigenvalues in the

ground state of the half-filled Landau level with short-range interactions and have found better agreement with the $\alpha = 2/3$ formula than with the $\alpha = 1$ one, which indicates a non-Fermi-liquid nature of the system. We have also found that our data tend to approach the $\alpha = 2/3$ formula with increasing N. This suggests an intriguing possibility that the COE and the physical heat capacity show the same power-law behavior in this strongly interacting metallic state.

The correspondence between the ES and the physical energy spectrum has been known in gapped topological phases [23,33–45] and in some gapless systems [48–51]. Our numerical result on the half-filled Landau level suggests that this correspondence also holds in a strongly interacting metallic state. It would be interesting to investigate whether this correspondence holds in other gapless systems with strong interactions. A calculation of the distribution of RDM eigenvalues would be useful for this purpose as the comparison with the analytical formula (8) allows us to efficiently probe the low-energy properties of the ES, as demonstrated in this paper. This contrasts with the strategies of Refs. [48–51], where the ES was compared with the known tower structure of the bulk energy spectrum; the use of the distribution of RDM eigenvalues does not require such prior knowledge. While the general condition for the correspondence between the ES and the physical spectrum is not known, the deviation of the COE or the distribution function from the $\alpha = 1$ behavior can already signal a non-Fermi-liquid nature, as explained in Sec. I. A particularly interesting class of systems to apply this idea are critical spin liquids with a spinon Fermi surface, as studied in Refs. [15,16], which are also considered to show heat capacity scaling as $T^{2/3}$ [78,79], similar to the half-filled Landau level.

ACKNOWLEDGMENTS

Y.O.N. thanks Y. Nakaguchi and T. Numasawa for valuable discussions. The authors thank Z. Papic for useful correspondence. The authors would like to thank the Yukawa Institute for Theoretical Physics at Kyoto University for hospitality during the long-term workshop YITP-T-16-01 "Quantum Information in String Theory and Many-body Systems" (May 2016), where part of our work was done. Y.O.N. was supported by the Advanced Leading Graduate Course for Photon Science (ALPS) of the Japan Society for the Promotion of Science (JSPS) and by JSPS KAKENHI Grant No. JP16J01135. S.F. was supported by JSPS KAKENHI Grant No. JP25800225 and the Matsuo Foundation.

APPENDIX A: $n_\alpha(\lambda)$ AS A SUM OF THE HYPERGEOMETRIC FUNCTION

When the exponent α of the COE is a rational number, the formula $n_\alpha(\lambda)$ for the cumulative distribution function in Eq. (8) can be written as a sum of the hypergeometric functions. In this appendix, we present explicit forms of such expressions.

The hypergeometric function is defined as

$$ {}_pF_q(\{a_1,\dots,a_p\};\{b_1,\dots,b_q\};x) = \sum_{k=0}^{\infty} \frac{(a_1)_k\cdots(a_p)_k}{(b_1)_k\cdots(b_q)_k}\frac{x^k}{k!}, \tag{A1}$$

where rising factorial $(a_i)_k$ is defined as $(a_i)_k := a_i(a_i+1)\cdots(a_i+k-1) = \Gamma(a_i+k)/\Gamma(a_i)$. When α equals an integer $m \in \mathbb{N}^+ = \{1,2,\dots\}$, one can show that Eq. (8) reduces to

$$ n_m(\lambda) = {}_0F_m\left(\{\};\left\{\frac{1}{m},\dots,\frac{m-1}{m},1\right\};\frac{x}{m^m}\right), \tag{A2}$$

where $x = b[\ln(\lambda_{\max}/\lambda)]^m$. When α is not an integer but a rational number, $\alpha = p/q$ (p and q are coprime integers), we observe that Eq. (8) can be written as the sum of the hypergeometric functions ${}_0F_M(gx^q)$, with $x = b[\ln(\lambda_{\max}/\lambda)]^\alpha$, where a rational number g and an integer M are determined from p and q. For example, when $\alpha = 2/3$, we obtain

$$\begin{aligned} n_{2/3}(\lambda) = {}&{}_0F_4\left(\{\};\left\{\frac{1}{3},\frac{1}{2},\frac{2}{3},1\right\};\frac{x^3}{108}\right) \\ &+\frac{x}{\Gamma\left(\frac{5}{3}\right)}{}_0F_4\left(\{\};\left\{\frac{2}{3},\frac{5}{6},\frac{4}{3},\frac{4}{3}\right\};\frac{x^3}{108}\right) \\ &+\frac{3x^2}{8\Gamma\left(\frac{4}{3}\right)}{}_0F_4\left(\{\};\left\{\frac{7}{6},\frac{4}{3},\frac{5}{3},\frac{5}{3}\right\};\frac{x^3}{108}\right), \end{aligned}$$

where $x = b[\ln(\lambda_{\max}/\lambda)]^{2/3}$.

APPENDIX B: TECHNICAL DETAILS OF NUMERICAL CALCULATIONS IN RELATIVISTIC FREE SCALAR BOSONS

In Sec. III A, we calculated the eigenvalues of a RDM for the ground state of relativistic free scaler bosons in two spatial dimensions. This calculation was based on the method of Ref. [73], and we here describe some technical details for completeness.

The field-theory action in a continuum is given by $S = \int d^2x dt[(\partial_t\phi)^2 - (\nabla\phi)^2]$. We decompose this action in terms of the angular momentum n and then discretize the radial direction into N points labeled by $i \in \{1,\dots,N\}$. Setting the lattice constant to unity, the resulting Hamiltonian is given by

$$ H = \frac{1}{2}\sum_{n=-\infty}^{\infty}\left(\sum_{i=1}^{N}\pi_{n,i}^2 + \sum_{i,j=1}^{N}\phi_{n,i}K_n^{i,j}\phi_{n,j}\right), $$

where $\phi_{n,i}$ and $\pi_{n,i}$ are the discretized scaler field and its conjugate field, respectively, for the angular momentum n and "site" i. The coefficients $K_n^{i,j}$ are given by $K_n^{1,1} = 3/2 + n^2$, $K_n^{i,i} = 2 + n^2/i^2$ ($i \geqslant 2$), $K_n^{i,i+1} = K_n^{i+1,i} = -(i+1/2)/\sqrt{i(i+1)}$, and $K_n^{i,j} = 0$ (otherwise).

We take as a subregion A a circle of radius R centered at the origin ($0 < R < N$). Since the theory is free (quadratic), the RDM of the ground state for subregion A can be written as a Gibbs state $\rho_A \propto \exp(-\sum_k \epsilon_k b_k^\dagger b_k)$, where $b_k^\dagger$ and b_k are some bosonic creation and annihilation operators. The single-particle "entanglement energy" ϵ_k can be calculated from eigenvalues of the correlation matrix C in the subregion A [80–82]. The correlation matrix C is defined through the correlation functions in the ground state as $C = \sqrt{XP}$, where $X_{i,j} := \otimes_n\langle\phi_{n,i}\phi_{n,j}\rangle_{GS}$ and $P_{i,j} := \otimes_n\langle\pi_{n,i}\pi_{n,j}\rangle_{GS}$ ($i,j = 1,\dots,R$). The eigenvalues of C, which we denote by ξ_k,

are related to ϵ_k as $\frac{1}{2}\coth(\epsilon_k/2) = \xi_k$. From ϵ_k, the many-body spectrum of ρ_A and the distribution function $n(\lambda)$ are calculated.

For the data presented in Fig. 1, we set $N = 40$ and $R = 10$. Since the correlation matrix C is block diagonalized in terms of the angular momentum n, ϵ_k can be calculated separately for different n. Since ϵ_k for large $|n|$ is generally small, we introduce a cutoff $n_{\max}$ for n in numerical calculations. We checked that the results do not change when we increase N or $n_{\max}$ while R/N is fixed.

[1] N. Laflorencie, Quantum entanglement in condensed matter systems, Phys. Rep. **646**, 1 (2016).

[2] L. Amico, R. Fazio, A. Osterloh, and V. Vedral, Entanglement in many-body systems, Rev. Mod. Phys. **80**, 517 (2008).

[3] M. Srednicki, Entropy and Area, Phys. Rev. Lett. **71**, 666 (1993).

[4] J. Eisert, M. Cramer, and M. B. Plenio, Colloquium: Area laws for the entanglement entropy, Rev. Mod. Phys. **82**, 277 (2010).

[5] C. Holzhey, F. Larsen, and F. Wilczek, Geometric and renormalized entropy in conformal field theory, Nucl. Phys. B **424**, 443 (1994).

[6] G. Vidal, J. I. Latorre, E. Rico, and A. Kitaev, Entanglement in Quantum Critical Phenomena, Phys. Rev. Lett. **90**, 227902 (2003).

[7] P. Calabrese and J. Cardy, Entanglement entropy and quantum field theory, J. Stat. Mech. (2004) P06002.

[8] P. Calabrese and J. Cardy, Entanglement entropy and conformal field theory, J. Phys. A **42**, 504005 (2009).

[9] M. M. Wolf, Violation of the Entropic Area Law for Fermions, Phys. Rev. Lett. **96**, 010404 (2006).

[10] D. Gioev and I. Klich, Entanglement Entropy of Fermions in Any Dimension and the Widom Conjecture, Phys. Rev. Lett. **96**, 100503 (2006).

[11] B. Swingle, Entanglement Entropy and the Fermi Surface, Phys. Rev. Lett. **105**, 050502 (2010).

[12] B. Swingle, Conformal field theory approach to Fermi liquids and other highly entangled states, Phys. Rev. B **86**, 035116 (2012).

[13] W. Ding, A. Seidel, and K. Yang, Entanglement Entropy of Fermi Liquids Via Multidimensional Bosonization, Phys. Rev. X **2**, 011012 (2012).

[14] J. McMinis and N. M. Tubman, Renyi entropy of the interacting Fermi liquid, Phys. Rev. B **87**, 081108 (2013).

[15] Y. Zhang, T. Grover, and A. Vishwanath, Entanglement Entropy of Critical Spin Liquids, Phys. Rev. Lett. **107**, 067202 (2011).

[16] T. Grover, Y. Zhang, and A. Vishwanath, Entanglement entropy as a portal to the physics of quantum spin liquids, New J. Phys. **15**, 025002 (2013).

[17] B. Swingle and T. Senthil, Universal crossovers between entanglement entropy and thermal entropy, Phys. Rev. B **87**, 045123 (2013).

[18] J. Shao, E.-A. Kim, F. D. M. Haldane, and E. H. Rezayi, Entanglement Entropy of the $\nu = 1/2$ Composite Fermion Non-Fermi Liquid State, Phys. Rev. Lett. **114**, 206402 (2015).

[19] R. V. Mishmash and O. I. Motrunich, Entanglement entropy of composite Fermi liquid states on the lattice: In support of the Widom formula, Phys. Rev. B **94**, 081110 (2016).

[20] H.-H. Lai and K. Yang, Probing critical surfaces in momentum space using real-space entanglement entropy: Bose versus Fermi, Phys. Rev. B **93**, 121109 (2016).

[21] N. Ogawa, T. Takayanagi, and T. Ugajin, Holographic Fermi surfaces and entanglement entropy, J. High Energy Phys. **01** (2012) 125.

[22] L. Huijse, S. Sachdev, and B. Swingle, Hidden Fermi surfaces in compressible states of gauge-gravity duality, Phys. Rev. B **85**, 035121 (2012).

[23] A. Kitaev and J. Preskill, Topological Entanglement Entropy, Phys. Rev. Lett. **96**, 110404 (2006).

[24] M. Levin and X.-G. Wen, Detecting Topological Order in a Ground State Wave Function, Phys. Rev. Lett. **96**, 110405 (2006).

[25] A. Hamma, R. Ionicioiu, and P. Zanardi, Bipartite entanglement and entropic boundary law in lattice spin systems, Phys. Rev. A **71**, 022315 (2005).

[26] A. Hamma, R. Ionicioiu, and P. Zanardi, Ground state entanglement and geometric entropy in the Kitaev model, Phys. Lett. A **337**, 22 (2005).

[27] M. A. Metlitski, C. A. Fuertes, and S. Sachdev, Entanglement entropy in the $o(n)$ model, Phys. Rev. B **80**, 115122 (2009).

[28] B. Hsu, M. Mulligan, E. Fradkin, and E.-A. Kim, Universal entanglement entropy in two-dimensional conformal quantum critical points, Phys. Rev. B **79**, 115421 (2009).

[29] J.-M. Stéphan, S. Furukawa, G. Misguich, and V. Pasquier, Shannon and entanglement entropies of one- and two-dimensional critical wave functions, Phys. Rev. B **80**, 184421 (2009).

[30] R. Islam, R. Ma, P. M. Preiss, M. E. Tai, A. Lukin, M. Rispoli, and M. Greiner, Measuring entanglement entropy in a quantum many-body system, Nature (London) **528**, 77 (2015).

[31] A. M. Kaufman, M. E. Tai, A. Lukin, M. Rispoli, R. Schittko, P. M. Preiss, and M. Greiner, Quantum thermalization through entanglement in an isolated many-body system, Science **353**, 794 (2016).

[32] H. Pichler, G. Zhu, A. Seif, P. Zoller, and M. Hafezi, Measurement Protocol for the Entanglement Spectrum of Cold Atoms, Phys. Rev. X **6**, 041033 (2016).

[33] H. Li and F. D. M. Haldane, Entanglement Spectrum as a Generalization of Entanglement Entropy: Identification of Topological Order in Non-Abelian Fractional Quantum Hall Effect States, Phys. Rev. Lett. **101**, 010504 (2008).

[34] R. Thomale, A. Sterdyniak, N. Regnault, and B. A. Bernevig, Entanglement Gap and a New Principle of Adiabatic Continuity, Phys. Rev. Lett. **104**, 180502 (2010).

[35] H. Yao and X.-L. Qi, Entanglement Entropy and Entanglement Spectrum of the Kitaev Model, Phys. Rev. Lett. **105**, 080501 (2010).

[36] A. M. Turner, Y. Zhang, and A. Vishwanath, Entanglement and inversion symmetry in topological insulators, Phys. Rev. B **82**, 241102 (2010).

[37] L. Fidkowski, Entanglement Spectrum of Topological Insulators and Superconductors, Phys. Rev. Lett. **104**, 130502 (2010).

[38] A. Sterdyniak, A. Chandran, N. Regnault, B. A. Bernevig, and P. Bonderson, Real-space entanglement spectrum of quantum Hall states, Phys. Rev. B **85**, 125308 (2012).

[39] J. Dubail, N. Read, and E. H. Rezayi, Real-space entanglement spectrum of quantum Hall systems, Phys. Rev. B **85**, 115321 (2012).

[40] X.-L. Qi, H. Katsura, and A. W. W. Ludwig, General Relationship Between the Entanglement Spectrum and the Edge State Spectrum of Topological Quantum States, Phys. Rev. Lett. **108**, 196402 (2012).

[41] A. Chandran, M. Hermanns, N. Regnault, and B. A. Bernevig, Bulk-edge correspondence in entanglement spectra, Phys. Rev. B **84**, 205136 (2011).

[42] J. Dubail, N. Read, and E. H. Rezayi, Edge-state inner products and real-space entanglement spectrum of trial quantum Hall states, Phys. Rev. B **86**, 245310 (2012).

[43] B. Swingle and T. Senthil, Geometric proof of the equality between entanglement and edge spectra, Phys. Rev. B **86**, 045117 (2012).

[44] R. Lundgren, Y. Fuji, S. Furukawa, and M. Oshikawa, Entanglement spectra between coupled Tomonaga-Luttinger liquids: Applications to ladder systems and topological phases, Phys. Rev. B **88**, 245137 (2013).

[45] J. Cano, T. L. Hughes, and M. Mulligan, Interactions along an entanglement cut in $2+1$D Abelian topological phases, Phys. Rev. B **92**, 075104 (2015).

[46] A. Chandran, V. Khemani, and S. L. Sondhi, How Universal is the Entanglement Spectrum? Phys. Rev. Lett. **113**, 060501 (2014).

[47] W. W. Ho, L. Cincio, H. Moradi, D. Gaiotto, and G. Vidal, Edge-entanglement spectrum correspondence in a nonchiral topological phase and Kramers-Wannier duality, Phys. Rev. B **91**, 125119 (2015).

[48] A. M. Läuchli, Operator content of real-space entanglement spectra at conformal critical points, arXiv:1303.0741.

[49] M. A. Metlitski and T. Grover, arXiv:1112.5166.

[50] V. Alba, M. Haque, and A. M. Läuchli, Entanglement Spectrum of the Two-Dimensional Bose-Hubbard Model, Phys. Rev. Lett. **110**, 260403 (2013).

[51] F. Kolley, S. Depenbrock, I. P. McCulloch, U. Schollwöck, and V. Alba, Entanglement spectroscopy of SU(2)-broken phases in two dimensions, Phys. Rev. B **88**, 144426 (2013).

[52] X. Chen and E. Fradkin, Quantum entanglement and thermal reduced density matrices in fermion and spin systems on ladders, J. Stat. Mech. (2013) P08013.

[53] J. Schliemann, Entanglement spectrum and entanglement thermodynamics of quantum Hall bilayers at $\nu = 1$, Phys. Rev. B **83**, 115322 (2011).

[54] J. Schliemann, Entanglement spectra and entanglement thermodynamics of Hofstadter bilayers, New J. Phys. **15**, 053017 (2013).

[55] J. Schliemann, Entanglement thermodynamics, J. Stat. Mech. (2014) P09011.

[56] Y. Nakaguchi and T. Nishioka, A holographic proof of Rényi entropic inequalities, J. High Energy Phys. 12 (2016) 129.

[57] This can be seen by following the logic of Sec. II inversely from Eq. (4).

[58] I. Affleck, Universal Term in the Free Energy at a Critical Point and the Conformal Anomaly, Phys. Rev. Lett. **56**, 746 (1986).

[59] P. Calabrese and Al. Lefevre, Entanglement spectrum in one-dimensional systems, Phys. Rev. A **78**, 032329 (2008).

[60] B. I. Halperin, P. A. Lee, and N. Read, Theory of the half-filled Landau level, Phys. Rev. B **47**, 7312 (1993).

[61] M. Barkeshli, M. Mulligan, and M. P. A. Fisher, Particle-hole symmetry and the composite Fermi liquid, Phys. Rev. B **92**, 165125 (2015).

[62] G. Murthy and R. Shankar, $\nu = \frac{1}{2}$, Phys. Rev. B **93**, 085405 (2016).

[63] D. T. Son, Is the Composite Fermion a Dirac Particle? Phys. Rev. X **5**, 031027 (2015).

[64] C. Wang and T. Senthil, Half-filled Landau level, topological insulator surfaces, and three-dimensional quantum spin liquids, Phys. Rev. B **93**, 085110 (2016).

[65] C. Wang and T. Senthil, Composite Fermi liquids in the lowest Landau level, Phys. Rev. B **94**, 245107 (2016).

[66] S. D. Geraedts, M. P. Zaletel, R. S. K. Mong, M. A. Metlitski, A. Vishwanath, and O. I. Motrunich, The half-filled Landau level: The case for Dirac composite fermions, Science **352**, 197 (2016).

[67] M. Levin and D. T. Son, Particle-hole symmetry and electromagnetic response of a half-filled Landau level, Phys. Rev. B **95**, 125120 (2017).

[68] C. Wang, N. R. Cooper, B. I. Halperin, and A. Stern, Particle-Hole Symmetry in the Fermion-Chern-Simons and Dirac Descriptions of a Half-Filled Landau Level, Phys. Rev. X **7**, 031029 (2017).

[69] Y. B. Kim and P. A. Lee, Specific heat and validity of the quasiparticle approximation in the half-filled Landau level, Phys. Rev. B **54**, 2715 (1996).

[70] P. Ruggiero, V. Alba, and P. Calabrese, Negativity spectrum of one-dimensional conformal field theories, Phys. Rev. B **94**, 195121 (2016).

[71] G. B. Mbeng, V. Alba, and P. Calabrese, Negativity spectrum in 1D gapped phases of matter, J. Phys. A **50**, 194001 (2017).

[72] I. R. Klebanov, S. S. Pufu, S. Sachdev, and B. R. Safdi, Rényi entropies for free field theories, J. High Energy Phys. 04 (2012) 074.

[73] Y. Nakaguchi and T. Nishioka, Entanglement entropy of annulus in three dimensions, J. High Energy Phys. 04 (2015) 072.

[74] Z. Liu and R. N. Bhatt, Evolution of quantum entanglement with disorder in fractional quantum Hall liquids, Phys. Rev. B **96**, 115111 (2017).

[75] F. D. M. Haldane, Fractional Quantization of the Hall Effect: A Hierarchy of Incompressible Quantum Fluid States, Phys. Rev. Lett. **51**, 605 (1983).

[76] S. A. Trugman and S. Kivelson, Exact results for the fractional quantum Hall effect with general interactions, Phys. Rev. B **31**, 5280 (1985).

[77] E. Rezayi and N. Read, Fermi-Liquid-Like State in a Half-Filled Landau Level, Phys. Rev. Lett. **72**, 900 (1994).

[78] M. Yu. Reizer, Relativistic effects in the electron density of states, specific heat, and the electron spectrum of normal metals, Phys. Rev. B **40**, 11571 (1989).

[79] D. F. Mross, J. McGreevy, H. Liu, and T. Senthil, Controlled expansion for certain non-Fermi-liquid metals, Phys. Rev. B **82**, 045121 (2010).

[80] I. Peschel, Calculation of reduced density matrices from correlation functions, J. Phys. A **36**, L205 (2003).

[81] I. Peschel and V. Eisler, Reduced density matrices and entanglement entropy in free lattice models, J. Phys. A **42**, 504003 (2009).

[82] H. Casini and M. Huerta, Entanglement entropy in free quantum field theory, J. Phys. A **42**, 504007 (2009).